Wind and Structures, Vol. 15, No. 3 (2012) 263-283
DOI: http://dx.doi.org/10.12989/was.2012.15.3.263

Lateral vibration control of a low-speed maglev vehicle in cross winds

J.D. Yau*[1,2]

[1]*Department of Transportation Management, Tamkang University, New Taipei City, Taiwan.*
[2]*College of Civil Engineering and Architecture, Zhejiang University, Hangzhou, China*

(Received October 2, 2010, Revised February 21, 2011, Accepted August 17, 2011)

Abstract. This paper presents a framework of nonlinear dynamic analysis of a low-speed moving maglev (magnetically levitated) vehicle subjected to cross winds and controlled using a clipped-LQR actuator with time delay compensation. A four degrees-of-freedom (4-DOFs) maglev-vehicle equipped with an onboard PID (Proportional-Integral-Derivative) controller traveling over guideway girders was developed to regulate the electric current and control voltage. With this maglev-vehicle/guideway model, dynamic interaction analysis of a low-speed maglev vehicle with guideway girders was conducted using an iterative approach. Considering the time-delay issue of unsynchronized tuning forces in control process, a clipped-LQR actuator with time-delay compensation is developed to improve control effectiveness of lateral vibration of the running maglev vehicle in cross winds. Numerical simulations demonstrate that although the lateral response of the maglev vehicle moving in cross winds would be amplified significantly, the present clipped-LQR controller exhibits its control performance in suppressing the lateral vibration of the vehicle.

Keywords: cross wind; incremental-iterative method; LQR actuator; maglev system; time delay

1. Introduction

Because of no physical contact for a maglev vehicle levitating on guide-rail, maglev transport system provides several advantages over conventional wheel/rail transportation for urban environment, such as low noise, less energy consumption, and low waste gas discharge. Thus, low-speed maglev transport system features its environmental-friendly nature to reduce traffic congestion and pollution in an urban travel. For these socioeconomic benefits, maglev technologies have been deployed in China, Japan, and Korea, for example, Shanghai Maglev Demonstration Line in China (Shi *et al*. 2007), Japanese Aichi low-speed Maglev transport system (Tobukyu Demonstration Line) for the "Aichi Expo. 2005" in Japan (Samavedam *et al.* 2002) and the urban maglev transport system (UTM-02) at Daejeon in Korea (Kwon *et al*. 2008).

Thanks to the advance of maglev technologies and application to transport system, two kinds of commercial maglev transportation have been developed: (1) the electrodynamic suspension (EDS) with repulsive mode (Bitta and Sales 1998); (2) the electromagnetic suspension (EMS) with attractive mode (Bohn and Steinmetz 1984). The EDS system suspends a train above its guide-rail

* Corresponding author, Professor, E-mail: jdyau@mail.tku.edu.tw

using magnetic repulsive forces to take the train off the U-shaped guideway. One feature of EDS-type maglev trains is that its magnetic levitation is workable only at high speeds. But the EMS system can lift a train up using attractive forces by the magnets between vehicle's levitation frame and guide-rail at any speed, which is the major difference from the EDS system.

In the past two decades, numerous researchers have focused on the dynamic problem of maglev vehicle-guideway interactions. Concerning the vehicle model of a maglev train running on a guideway, Cai *et al.* (1996) pointed out that a concentrated-load vehicle model might gives rise to larger response on both guideway deflections and vehicle accelerations than a distributed-load vehicle model. In addition, Cai and Chen (1997) provided a literature review for various aspects of the dynamic characteristics, magnetic suspension systems, vehicle stability, suspension control laws of maglev/guideway coupling systems. Zheng *et al*. (2000, 2005) developed two kinds of maglev vehicle/guideway coupling models to investigate the dynamic problems of divergence, flutter, and collision on the dynamic stability of a maglev-vehicle traveling on a flexible guideway. Song and Fujino (2008) modeled the levitation and guidance forces between the super-conducting magnet and guideway using an equivalent spring to investigate the dynamic responses of ultra high-speed Maglev train-guideway interactions. Yau (2009a, 2009b, 2010a,b,c) and Yang and Yau (2011) carried out a series of dynamic investigations of maglev vehicles traveling over flexible guideways. Their research topics on interaction dynamics of maglev transport system included vibration control of moving vehicle, vehicle-guideway/soil-foundation interactions, influence of ground settlement on moving maglev vehicles, earthquakes induced vibrations vehicle/guideway system, and vibrations of a high speed maglev vehicle under oncoming wind flows.

On the other hand, a great deal of attention has been focused on the aerodynamics of conventional trains in the past one decade, such as train-induced aerodynamic vibrations (Li *et al.* 2005), cross wind effects on vehicle-bridge interaction (Suzuki *et al.* 2003, Xu *et al*. 2004, Bocciolone, *et al*. 2008, Xia *et al*. 2008, Guo *et al*. 2010), and impulse side forces occurring at trains passing by each other (Fujii and Ogawa 1995). Recently, Kwon *et al*. (2008) investigated the vibration behaviors of a maglev vehicle running over a suspended guideway under wind loadings. Considering oncoming aerodynamic forces applying to a maglev vehicle moving at high speeds, Yau (2010c) presented a PID+LQR controller to reduce the vehicle's acceleration response for ride comfort of passengers. Their numerical simulations demonstrated that aerodynamic forces play a dominant issue in affecting the response of a maglev vehicle running over (suspended) guideways at high speeds. However, to the author's knowledge, relatively little research attention so far seems to conduct lateral vibration of a low-speed maglev vehicle in cross winds, especially for the lateral vibration control problem.

As shown in Fig. 1, a low speed maglev vehicle is traveling over a series of guideway girders in cross wind environment. In this study, the maglev vehicle is simulated as a rigid car body supported and guided by four concentrated magnetic levitation forces and the guideway girder is modeled as a

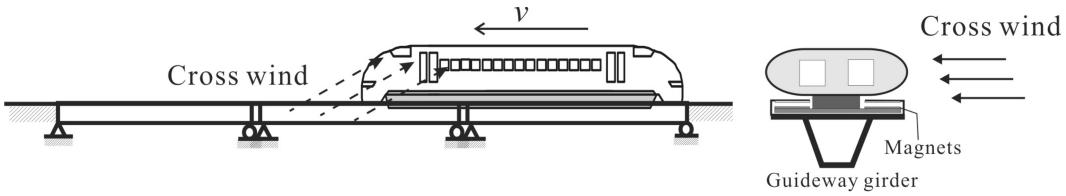

Fig. 1 Schematic diagram of a maglev vehicle moving over guideway girders in cross winds.

simply supported beam. To explore the influence of cross winds on interaction response of the maglev-vehicle/guideway system, this study adopts an optimal PID controller with *constant* tuning gains based on Z-N tuning rule associated with clipped-LQR controller with time delay compensation (Ni *et al*. 2002, Lee and Kawashima 2007) to regulate the lateral levitation forces exerting on the moving maglev vehicle. Then the two sets of differential equations associated with the equations of control electromagnetic forces for the maglev vehicle/guideway system are solved by Galerkin's method and computed using an iterative approach (Yau 2009a,b,c) associated with the Newmark method (1959). Numerical studies indicate that although cross wind loadings may result in a significant amplification of the lateral response of the running maglev vehicle, the present clipped-LQR control algorithm exhibits its superiority in reducing lateral response of the vehicle.

2. Governing equations of motion

From the research presented by Cai *et al*. (1996), they pointed out that a distributed-load vehicle model behaves better than a concentrated-load model in both responses of guideway and vehicles. For this reason, the maglev vehicle supported by multiple magnetic wheels is employed to conduct the dynamic behavior of a low-speed maglev vehicle/guideway transport system in this study. Since this paper is focused on the lateral vibration control of a moving maglev vehicle under cross winds, for the problem simplifications, wide magnets below the levitation frame (see Fig. 1) would be designated to increase the lateral stability of the car body against aerodynamic rolling moments. Thus, the aerodynamic rolling moments exerting to the moving maglev vehicle would be assumed relatively small and negligible. The following are the assumptions adopted for the present maglev vehicle/guideway model: (1) The guideway system is modeled as a series of simply supported beams with identical properties and the beam is idealized as a linear elastic Bernoulli-Euler beam with uniform section; (2) The maglev vehicle is simulated as a *rigid* beam supported and guided by four magnetic forces; (3) Allowable levitation gap (h) at the magnetic wheel should not contact with the guide rail, i.e., $h > 0$; (4) The magnets below the levitation frame (see Fig. 1) are regarded as a series of equal-distant concentrated masses attached to the rigid beam; (5) The influence of shape of guideway girders on aerodynamic coefficients of a moving vehicle is negligible because only short-span girder is considered.

As shown in Fig. 2, a maglev vehicle supported by four magnet wheels with equal-intervals (d) is passing through a series of simple beams at constant speed v. Here, we shall use the following symbols to denote the properties depicted in the schematic diagram of Fig. 2: m = distributed mass of the beam, c = damping coefficient, EI_y = flexural rigidity in the y direction, EI_z = flexural rigidity in the z direction, l = car length, m_w = lumped mass of magnetic wheel, m_v = distributed mass of the rigid car body, and $\theta_i\big|_{i=y,z}$ n = midpoint rotation components of the rigid car body. Then, one can formulate the equations of motion for the jth guideway girder carrying a moving maglev vehicle suspended by multiple magnetic forces as follows

$$\begin{aligned} m\ddot{u}_{y,j} + c_y\dot{u}_{y,j} + EI_z u''''_{y,j} &= -\sum_{k=1}^{K}[G_{y,k}\varphi_j(x,t)] \\ m\ddot{u}_{z,j} + c_z\dot{u}_{z,j} + EI_z u''''_{y,j} &= p_o - \sum_{k=1}^{K}[G_{z,k}\varphi_j(x,t)] \end{aligned} \tag{1}$$

and

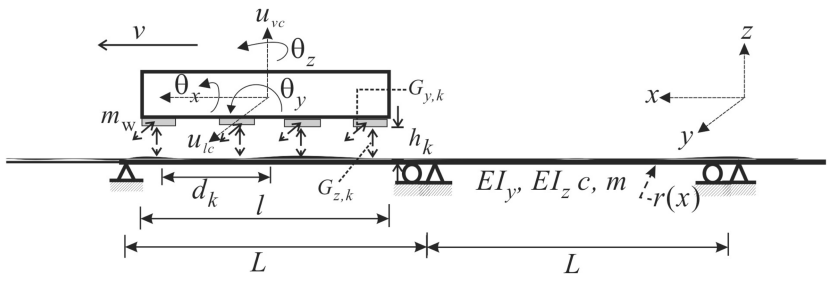

Fig. 2 Mathematical model of a maglev vehicle running on a series of simple beams.

$$\varphi_j(x,t) = \delta(x-x_k)\left[H\left(t-t_k-\frac{(j-1)L}{v}\right)-H\left(t-t_k-\frac{jL}{v}\right)\right] \tag{2}$$

together with the following boundary conditions

$$\begin{aligned} u_{y,j}(0,t) &= u_{z,j}(0,t) = 0 \\ u_{y,j}(L,t) &= u_{z,j}(L,t) = 0 \\ EI_z u''_{y,j}(0,t) &= EI_z u''_{y,j}(0,t) = 0 \\ EI_z u''_{y,j}(L,t) &= EI_y u''_{z,j}(L,t) = 0 \end{aligned} \tag{3}$$

where $(\bullet)' = \partial, (\bullet)/\partial x, (\dot{\bullet}) = \partial(\bullet)/\partial t, u_{z,j}(x,t)$ vertical deflection of the jth span, $u_{y,j}(x,t)$ = lateral deflection of the jth span, L = span length, K = number of magnetic wheel-sets attached to the rigid levitation frame, $\delta(\bullet)$ = Dirac's delta function, $H(t)$ = unit step function, k = 1, 2, 3, …, Kth moving magnetic wheel on the beam, $t_k = (k-1)d/v$ = arrival time of the kth magnetic wheel into the beam, x_k = position of the K-th magnetic wheel on the guide-way, and ($G_{y,k}$, $G_{z,k}$) = lateral guidance and uplift levitation forces of the kth lumped magnet in the vertical and lateral directions.

As a maglev vehicle moves over a guideway in cross winds, wind-induced lateral movement would result in considerable influence on riding comfort and maneuverability of the levitated vehicle. For this reason, guidance forces induced by the maglev system need to control the lateral motion of the moving maglev vehicle. For the kth lumped magnetic wheel of the moving maglve vehicle, this study adopts the uplift levitation force ($G_{z,k}$) and lateral guidance force ($G_{y,k}$) proposed by Aldo and Alfred (1999) to keep and guide the maglev vehicle moving on the guideway girders. They are expressed as

$$G_{y,k} = \kappa_0\left(\frac{i_k}{h_{z,k}}\right)^2\left(1-\frac{\chi_k \times h_{z,k}}{W(1+\chi_k)}\right) \tag{4a}$$

$$G_{z,k} = \kappa_0\left(\frac{i_k}{h_{z,k}}\right)^2\left(1-\frac{\chi_n \times h_{y,k}}{W(1+\chi_k)}\right) \tag{4b}$$

where $\chi_k = \pi h_{y,k}/4h_{z,k}$, W = pole width, $\kappa_0 = \mu_0 N_0^2 A_0/4$ = coupling factor, μ_0 = vacuum permeability, N_0 = number of turns of the magnet windings, A_0 = pole face area, $i_k(t) = i_0 + \iota_k(t)$ = control current, $\iota_k(t)$ = deviation of control current, and (i_0, h_{y0}, h_{z0}) = desired control current and

levitation gaps around a specified nominal operating point of the maglev wheels at *static* equilibrium. The corresponding levitation gaps in lateral and vertical directions are respectively given by

$$\begin{aligned} h_{y,k}(t) &= h_{y0} + u_{t,k}(x_k), \qquad u_{l,k}(t) = u_{lc}(t) + d_k\theta_{zk} \\ h_{z,k}(t) &= h_{z0} + u_{v,k}(t) - u_{z,j}(x_k) + r(x_k), \qquad u_{v,k}(t) = u_{vc}(t) + d_k\theta_{yk} \end{aligned} \tag{5}$$

where ($u_{l,k}$, $u_{v,k}$) = displacements of the kth magnetic wheel in the y and z directions, (u_{lc}, u_{vc}) = midpoint displacements of the rigid car, (θ_y, θ_z) = midpoint rotations of the rigid car, $r(x)$ = irregularity of guideway, and d_k = location of the kth magnetic wheel to the midpoint of the rigid beam. Observing the expression of Eq. (4), the increase of lateral air gaps would increase the lateral force but decrease the uplift levitation force of the maglev system. From the electromagnetic forces expressed in Eq. (4), the motion-dependent nature of magnetic force plays a key role to resolve the dynamic problem of maglev vehicle-guideway interaction tuned by a maglev system. On the other hand, the equations of motion of a 4-DOFs (see Fig. 2) maglev vehicle with rigid car body are given by

$$\begin{aligned} M_0\ddot{u}_{lc} &= g(t) + F_S + \sum_{k=1}^{K} G_{y,k}, \quad I_T\ddot{\theta}_z = M_P + \sum_{k=1}^{K}[G_{y,k}d_k] \\ M_0\ddot{u}_{vc} &= -p_0 + F_L + \sum_{k=1}^{K} G_{z,k}, \quad I_T\ddot{\theta}_y = M_Y - \sum_{k=1}^{K}[G_{z,k}d_k] \end{aligned} \tag{6}$$

in which $M_0 = m_v l + Km_w$ = lumped mass of the vehicle, $g(t)$ denotes the feedback gain to control the lateral response of the maglev vehicle, I_T = mass moment of inertia of the rigid car body, $p_0 = M_0 g$ = lumped weight of the maglev vehicle, (F_S, F_L) = aerodynamic side and lift forces, and (M_P, M_Y) = aerodynamic pitching and yawing moments.

3. Lateral vibration control of a maglev vehicle using LQR actuator

In vibration control theory, LQR algorithm has been widely used in optimal control for its simplicity, reliability, robustness, and stability in a closed-loop system (Soong 1990). This paper is aimed at investigating the lateral vibration control of a moving maglev vehicle under cross winds. Thus, the equation of lateral component for the maglev vehicle in Eq. (6) can be rewritten as

$$\begin{aligned} M_0\ddot{u}_{lc} &= g(t) + f(t) \\ f(t) &= F_S + \sum_{k=1}^{K}[G_{y,k}] \end{aligned} \tag{7}$$

Introducing the state space of $\langle y \rangle = \langle u_{lc} \quad \dot{u}_{lc} \rangle$ into Eq. (7) yields the following matrix equation

$$\{\dot{y}\} = [A]\{y\} + \{B\}g(t) + \{C\}f(t)$$

$$[A] = \begin{bmatrix} 0 & 1 \\ 0 & 0 \end{bmatrix}, \ \{B\} = \begin{Bmatrix} 0 \\ 1/M_0 \end{Bmatrix}, \ \{C\} = \begin{Bmatrix} 0 \\ 1/M_0 \end{Bmatrix}, \ g(t) = [G]\{y\} \tag{8}$$

where $\{y\} = \langle y \rangle^T$ and $[G]$ represents the control gain matrix. In this control algorithm, the control gain $g(t)$ is determined by minimizing the following quadratic cost index (Soong 1990)

$$J = \int_0^{t_f} [\{y\}^T [Q] \{y\} + Rg^2] dt \tag{9}$$

Here, $[Q]$ is a symmetric positive semi-definite weighting matrix for the performance of a structural system and R the weighting parameter for the input control force. To minimize the performance index J in Eq. (9), the Riccati equation (Soong 1990) is usually used to obtain the Riccati matrix $[P]$ and the control gain matrix $[G]$, i.e.

$$[P][A] - \frac{1}{2}[P]\{B\}R^{-1}\{B\}^T[P] + [A]^T[P] + 2[Q] = [0] \tag{10}$$

$$[G] = \frac{-1}{2}R^{-1}[B]^T[P] \tag{11}$$

In this study, the weighting matrix $[Q]$ is represented by

$$[Q] = \begin{bmatrix} k_w & 0 \\ 0 & 0 \end{bmatrix} \tag{12}$$

where k_w is weighting parameter. The solution of the Riccati matrix $[P]$ and the corresponding control gain $g(t)$ in Eq. (8) are derived from (Yau 2010c), they are expressed as

$$[P] = 2M_0 \begin{bmatrix} \sqrt{\sqrt{k_w/R} \times k_w/M_0} & \sqrt{k_w R} \\ \sqrt{k_w R} & \sqrt{2M_0 R \sqrt{k_w R}} \end{bmatrix} \tag{13}$$

$$g(t) = [\mathrm{G}]\{z\} = -(\sqrt{2M_0\sqrt{k_w/R}} \times \dot{u}_v + \sqrt{k_w/R} \times u_v) \tag{14}$$

Let $R = k_w/\Psi^2$, the coefficient Ψ represents the relative importance of control performance in response suppression (Soong 1990). Introducing the derived control force $g(t)$ shown in Eq. (14) into Eq. (7) yields

$$M_0\ddot{u}_{lc} + \sqrt{2M_0\Psi \times \dot{u}_{lc}} + \Psi u_{lc} = F_S + \sum_{k=1}^{K}[G_{y,k}] \tag{15}$$

3.1 Determination of coupling factor

From the condition of static equilibrium for the suspended maglev vehicle with initial gaps of h_{y0} and h_{z0}, one can obtain the following *static* electromagnetic force at the k-th magnetic wheel from Eq. (4)

$$G_{y0} = \kappa_0 \gamma_{z0}^2 \left[\frac{\chi_0 \times h_z/W}{1+\chi_0}\right], \; G_{z0} = \kappa_0 \gamma_{z0}^2 \left[1 - \frac{\chi_0 \times h_{y0}/W}{1+\chi_0}\right] = \frac{p_0}{K} \tag{16}$$

Here, $\gamma_{z0} = i_0/h_{z0}$ and $\chi_0 = \pi h_{y0}/4h_{z0}$. To keep the maglev vehicle in static equilibrium at initial lateral air gap of h_{y0}, the control force required for the LQR actuator can be represented by

$$\Psi_0 h_{y0} = \sum_{k=1}^{K} [G_{y0}] \tag{17}$$

where Ψ_0 means the initial stiffness parameter tuned by the LQR actuator. Solving Eqs. (16) and (17) yields the following initial parameters

$$\kappa_0 = \frac{p_0 \gamma_{z0}^{-2}}{2K}\left[1 - \frac{\chi_0 \times h_{y0}/W}{1+\chi_0}\right]^{-1}, \quad \Psi_0 = \frac{\pi p_0/4\mathrm{W}}{1+(1-h_{y0}/W)\chi_0} \tag{18}$$

For the special case of $h_{y0} = 0$, the coupling factor becomes $\kappa_0 = p_0/K\gamma_{z0}^2$, which is reduced to the case of a maglev vehicle at vertical static equilibrium without initial lateral movement (Yau 2009a,b).

As a maglev vehicle moves over guideway in cross winds, the control actuator needs to provide additional gain for tuning the controller, let $\Psi = \Psi_0 + \psi$ and consider the initial lateral air gap of h_{y0}, thus, the equation of lateral motion for the moving maglev vehicle becomes

$$M_0 \ddot{u}_{lc} + \sqrt{2M_0(\Psi_0+\psi)} \times \dot{u}_{lc} + (\Psi_0+\psi)u_{lc} = F_S - \Psi_0 h_{y0} + \sum_{k=1}^{K}[G_{y,k}] \tag{19}$$

Here, ψ represents additional tuning stiffness gain as the maglev vehicle runs on the guideway under cross wind environments. In this paper, ψ is set $\Psi_0/10$.

3.2 Clipped LQR control

If the control force $g(t)$ of the LQR controller is bounded by a maximum value f_{max}, the controller with *saturated* tuning gain can be simulated by a variable damper (Ni *et al*. 2004, Lee and Kawashima 2007). Thus the equation of lateral motion of the maglev vehicle in Eq. (19) is rewritten as

$$\begin{aligned} M_0 \ddot{u}_{lc} + c_d \dot{u}_{lc} + \Psi_0 u_{lc} &= F_S - \Psi_0 h_{y0} + \sum_{k=1}^{K}[G_{y,k}] \\ c_d(t) &= \frac{-\hat{g}(t)}{\dot{u}_{lc}(t)} \end{aligned} \tag{20}$$

where c_d = variable damping coefficient and $\widehat{g}(t)$ = saturated control gain. Based on the clipping control strategy (Ni *et al*. 2004, Lee and Kawashima 2007), the saturated control gain $\widehat{g}(t)$ in Eq. (20) is expressed as

$$\widehat{g}(t) = \begin{cases} sgn[g(t)] \times f_{\max} & g(t)\dot{u}_{lc} > 0 \ \text{ and } \ |g(t)| > f_{\max} \\ g(t)[= (-\sqrt{2M_0\Psi} \times \dot{u}_{lc} - \psi u_{lc})] & (g(t)\dot{u}_{lc} < 0 \ ) \text{and } \ (|g(t)| < f_{\max}) \\ 0 & \text{otherwise} \end{cases} \tag{21}$$

Here, sgn[$g(t)$] means the sign function of the control gain $g(t) = (-\sqrt{2M_0\Psi}\dot{u}_{lc} - \Psi u_{lc})$. It is emphasized that the variable damping coefficient $c_d(t)$ not only behaves like a semi-active controller to tune its control gain from the lateral feedback responses of $(u_{lc}, \dot{u}_{lc})$ of the running maglev vehicle but also functions as a conventional LQR controller to control the lateral vibration of the running maglev vehicle. In this paper, the maximum saturated control gain of $f_{\max}$ =

$0.8 \times |g(t)|_{\max}$ is selected as the upper bound of control forces. Here, $|g(t)|_{\max}$ represents the absolute maximum control force computed from the running maglev vehicle without clipping control.

3.3 Compensation of time-delayed system

As shown in Eq. (14), it is a control force of an ideal control actuator without time delay. In reality, time delay is an important issue degrading control effectiveness of a controlled structure and exists between the response measurement and the control action, which may result in unsynchronized control forces exerting to the controlled structure. Thus time delay issue cannot be avoided in an entire control process. To alleviate the degradation of control performance due to time delays, this study employs the phase-shift compensation method (Symans and Constantinou 1997) to improve the control effectiveness of the present LQR actuator with time delay. Let us denote τ as the time delay between response measurement and control action. Then the actual control force $g(t)$ without compensation exerting to the vehicle in lateral direction is

$$g(t) = -\Psi \times u_{lc}(t-\tau) - \sqrt{2M_0\Psi} \times \dot{u}_{lc}(t-\tau) \tag{22}$$

Based on the phase-shift compensation method (Symans and Constantinou 1997, Agrawal and Yang 2000), the feedback parameters of the time-delayed controller can be appropriately modified from the real control gain $g(t)$ such that the time-delayed system have the same tuning stiffness (Ψ) and damping ($\sqrt{2M_0\Psi}$) parameters as the ones of the ideal controller, that is

$$g(t) = -g_v \times \dot{u}_{lc}(t-\tau) - g_d \times u_{lc}(t-\tau) \tag{23}$$

where the modified feedback parameters (g_v, g_d) were given by the following transformation (Symans and Constantinou 1997)

$$\begin{Bmatrix} g_d \\ g_v \end{Bmatrix} = \begin{bmatrix} \cos(\omega\tau) & \omega(\sin(\omega\tau)) \\ -\sin(\omega\tau)/\omega & \cos(\omega\tau) \end{bmatrix} \begin{Bmatrix} \Psi \\ \sqrt{2M_0\Psi} \end{Bmatrix} \tag{24}$$

where $\omega(=\sqrt{\Psi_0/M_0})$ is the lateral natural frequency of the controlled maglev vehicle at static equilibrium.

4. Control equation of the maglev suspension system

By the theory of electromagnetic circuits, the electromagnetic equation of magnet current and control voltage for the kth electric magnets in the maglev suspension system is given by

$$\Gamma_0 \frac{d(i_k/h_{z,k})}{dt} + R_0 i_k - V_k \tag{25}$$

where $\Gamma_0 = 2\kappa_0$ = initial inductance of the coil winding the suspension magnet, R_0 = coil resistance of electronic circuit, and V_k = control voltage. To control the levitation forces between the mgalev vehicle and guideway, an onboard PID control algorithm (Astrom and Hagglund 1988) is

employed to regulate control voltage of the maglev system. Let us adopt the variable transformation as $\gamma_{zk} = i_k/h_{z,k}$, the control voltage V_k can be expressed in terms of error function of $e_k(= i_0/h_{z0} - i_k/h_{z,k} = \gamma_{z0} - \gamma_{zk})$ in the control process by using PID tuning algorithm as (Ogata 1997)

$$V_k = K_p e_k + K_i \int_0^t e_k dt + K_d \dot{e}_k \tag{26}$$

where K_p = proportional gain, K_i = integral gain, and K_d = derivate gain. Then substituting Eq. (26) into Eq. (25) and differentiating this equation with respect to time, one can achieve the following differential equation for control error function

$$(\Gamma_0 + K_d)\ddot{e}_k + (K_p + R_0 h_{zk})\dot{e}_k + (K_i + R_0 \dot{h}_{zk})e_k - R_0\gamma_{z0}(\dot{u}_{vc} - d_k\dot{\theta}_y) = R_0\gamma_{z0}(\dot{r}(x_k) - \dot{u}_{zj}) \tag{27}$$

With the aid of control error function e_k and the parameter $\gamma_{z0} = i_0/h_{z0}$ at static equilibrium, the equations of motion in Eq. (6) for the controlled maglev vehicle can be rewritten as

$$\begin{aligned}
M_0\ddot{u}_{lc} + c_b \times \dot{u}_{lc} + \Psi_0 u_{lc} &= F_S - \Psi_0 h_{y0} + \Upsilon_0 \sum_{k=1}^{K} \left[\left(\frac{e_k}{\gamma_{z0}} - 1\right)^2 \left[\frac{h_{z,k}^2 \chi_k / W}{h_{z,k}(1+\chi_n)}\right]\right] \\
I_y\ddot{\theta}_z &= M_Y + \Upsilon_0 \sum_{k=1}^{K} \left[\left(\frac{e_k}{\gamma_{z0}} - 1\right)^2 \left[\frac{h_{z,k}^2 \chi_k / W}{h_{z,k}(1+\chi_n)}\right] d_k\right] \\
M_0\ddot{u}_{vc} &= -p_0 + F_L + \Upsilon_0 \sum_{k=1}^{K} \left(\frac{e_k}{\gamma_{z0}} - 1\right)^2 \left[1 - \frac{\chi_k \times h_{y,k}}{W(1+\chi_k)}\right] \\
I_T\ddot{\theta}_y &= M_P + \Upsilon_0 \sum_{k=1}^{K} \left[\left(\frac{e_k}{\gamma_{z0}} - 1\right)^2 \left[1 - \frac{\chi_k \times h_{y,k}}{W(1+\chi_k)}\right] d_k\right]
\end{aligned} \tag{28}$$

where

$$\Upsilon = \frac{(1+\chi_0)p_0/K}{1 + \chi_0(1 - h_{y0}/W)} \tag{29}$$

Then the combination of Eqs. (27) and (28) yields the following equations of motion for the maglev vehicle equipped with an onboard controller

$$[m_v]\{\ddot{u}_v\} + [c_{v,k}]\{\dot{u}_v\} + [k_v]\{u_v\} = \{f_v\} \tag{30}$$

in which $\{u_v\}$ = displacement vector, $\{f_v\}$ = force vector, and ($[k_v]$, $[c_v]$, $[m_v]$) means structural matrices of the maglev vehicle.

5. Simulation of turbulent wind velocity

In general, the simulation of turbulent wind loads acting on a moving maglev vehicle is usually

obtained from the numerical interpolation of the turbulent wind loads of the guideway girder at the two adjacent monitoring nodes (Xu *et al*. 2004, Xia *et al*. 2008). To perform the interaction analysis of a maglev vehicle traveling over guideway under cross winds in the time domain, the following simplified spectral representation of turbulent wind (Cao *et al*. 2000) is employed to generate the time history of horizontal turbulent airflow velocity $w_j(t)$ in mean wind flow direction at the jth point on the guideway system as

$$w_j(t) = \sqrt{2(\Delta\omega)}\sum_{n=1}^{j}\left[\sum_{i=1}^{N_f}\sqrt{S(\omega_{ni})}\times G_{jn}(\omega_{ni})\times\cos(\omega_{ni}t+\upsilon_{ni})\right], j = 1, 2, \ldots, N_s \tag{31}$$

where N_f is the total number of frequency intervals represented by a sufficiently large number; N_s is the total number of points along the guideway to simulate; S(ω) is the horizontal spectral density of turbulent wind; υ_{ni} is a random variable uniformly distributed between 0 and 2π, $\Delta\omega = \omega_{up}/N_f$ the frequency increment; ω_{up} is the upper cutoff frequency with the condition that the value of wind spectrum is less than a preset small number ε when $\omega > \omega_{up}$. The spectrum formula shown in Eq. (31) for horizontal turbulent wind velocity is defined by

$$S(\omega) = \frac{200\times\overline{U}^2}{[1+50f(z)]^{5/3}}\left(\frac{z}{U}\right),\ f(z) = \frac{\omega}{2\pi}\frac{z}{U} \tag{32}$$

$$G_{jn}(\omega) = \begin{cases} 0 & 1\le j<n\le N_s \\ C^{|j-n|} & n=1, n\le j\le N_s, \\ C^{|j-n|}\sqrt{1-C^2} & 2\le n\le j\le N_s \end{cases} \qquad C = \exp\left(\frac{-\lambda\omega\times l_{jn}}{2\pi U}\right) \tag{33}$$

where $\overline{U}$ stands for the shear velocity of airflow; U is the mean wind speed at height z; λ is an exponential decay factor taken between 7 and 10; l_{jn} is the distance between the simulated points j and n; and $C^{|j-n|}$ is the coherence function between points j and n (Cao *et al*. 2000, Xia *et al*. 2008).

5.1 Simulation of quasi-steady aerodynamic forces on the moving vehicle

Fig. 3 shows the wind load model acting on the running vehicle with a mean velocity U and turbulent velocity w. The *aerodynamic forces* and *moments* acting at the mass center of the moving vehicle are expressed as

$$\begin{aligned} F_s &= \frac{\rho A_S U_r^2}{2}C_S(\varphi),\ M_Y = \frac{\rho A_S d_e U_r^2}{2}C_Y(\varphi) \\ F_L &= \frac{\rho A_T U_r^2}{2}C_L(\varphi),\ M_P = \frac{\rho A_T h_v U_r^2}{2}C_M(\varphi) \\ U_r &= \sqrt{[v+U\cos\phi]^2+[(U+w)\sin\phi]^2} \\ \tan\varphi &= \frac{(U+w)\sin\phi}{v+U\cos\phi} \end{aligned} \tag{34}$$

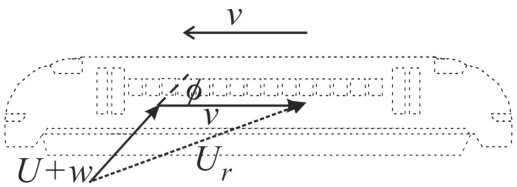

Fig. 3 Relative wind velocity and natural wind velocity to a moving vehicle.

where ρ is the air density (= 1.2kg/m^3); A_S is the side surface area of the vehicle; A_T is the top surface area of the vehicle; d_e is the reference eccentricity of aerodynamic yawing moment about the mass center; h_v is the reference height of vehicle's mass center; C_S is aerodynamic coefficient of vehicle's side; C_L is aerodynamic lift coefficient; C_P is aerodynamic pitching moment coefficient; ϕ(= arctan(U/v)) is yaw angle (see Fig. 2); U_r is the *relative* wind velocity around the vehicle moving at speed v; and w represent the turbulent wind speed component defined in Eq. (31).

6. Method of solution

As the beam equation shown in Eqs. (1) and (3), it is a differential equation associated with non-homogeneous boundary conditions. The deflection response $u_j(x,t)$ can be expressed as

$$u_{y,j}(x,t) = \sum_{n=1} q_{y,jn}(t)\sin\frac{n\pi x}{L},\ u_{z,j}(x,t) = \sum_{n=1} q_{z,jn}(t)\sin\frac{n\pi x}{L} \tag{35}$$

Here, $q_{jn}(t)$ means the generalized coordinate associated with the nth vibration mode of the jth span. By Galerkin's method (Yau 2009a,b,c), the generalized equation of motion for the nth modal system of the jth beam becomes

$$\begin{aligned} m\ddot{q}_{y,jn} + c_{y,n}\dot{q}_{y,n} + m\omega^2 q_{y,jn} &= p_{y,jn} \\ m\ddot{q}_{z,jn} + c_{z,n}\dot{q}_{y,n} + m\omega_{zn}^2 q_{z,jn} &= p_{z,jn} \\ \omega_{y,n} = \left(\frac{n\pi}{L}\right)^2\sqrt{\frac{EI_z}{m}},\ \ \omega_{z,n} &= \left(\frac{n\pi}{L}\right)^2\sqrt{\frac{EI_y}{m}} \end{aligned} \tag{36}$$

where ($c_{y,n}$, $c_{z,n}$) = the nth modal damping coefficient, and ($\omega_{y,n}$, $\omega_{z,n}$) = the nth natural frequency, and thegeneralized magnetic forces are given by

$$\begin{aligned} p_{y,jn} &= \frac{2}{L}\sum_{k=1}^{K}[G_{y,k}\Phi_{jn}(t)],\ p_{z,jn} = \frac{2}{L}\sum_{k=1}^{K}\left[\left(-\frac{p_0}{K} + G_{z,k}\right)\Phi_{jn}(t)\right] \\ \Phi_{jn}(t) &= sin\frac{n\pi v}{L}(t-t_k)\times\left[H\left(t-t_k-\frac{(j-1)}{v}\right) - H\left(t-t_k-\frac{jL}{v}\right)\right] \end{aligned} \tag{37}$$

7. Applications of the incremental-iterative approach

Because of the motion-dependent and non-contact nature of electromagnetic forces, the nonlinear dynamic analysis of the maglev vehicle/guideway system needs to be solved by iterative method. The numerical procedure of incremental-iterative dynamic analysis conventionally involves three phases: *predictor*, *corrector,* and *equilibrium checking* (Yang and Kuo 1994). Detailed information about the incremental-iterative procedure for nonlinear dynamic analysis of vehicle-bridge interaction is available in references (Yau 2009a,b, 2010a,b,c). Fig. 4 shows the analysis flow chat to carry out the nonlinear dynamic analysis for the vibration control and interaction responses of maglev vehicle/guideway system in cross winds. It is noted that (1) The structure matrices in Eq. (30) for the dynamic interactions of maglev vehicle/guideway system should be updated at each iteration; (2) The root mean square β_{tol} of the sum of unbalanced forces for the maglev vehicle/guideway interaction system, that is

$$\beta_{tol} = [\ \sum_{k=1\ldots}^{K} (\Delta f_{vk+\Delta t}^{\,i-1})^2 + \sum_{n=1} (\Delta p_{n,\,t+\Delta t}^{\,i-1})^2\ ]^{1/2} \tag{38}$$

is larger than a preset tolerance, say 10^{-3}, iteration for removing the unbalanced forces involving the two phases of predictor and corrector should be repeated. Here, $\Delta p_{n,\,t+\Delta t}^{\,i-1}$ = the unbalanced force between the external force $p_{n,\,t+\Delta t}^{\,i-1}$ and the effective internal forces $f_{n,\,t+\Delta t}^{\,i-1}$ for the n-th generalized system at the i-th iteration of time $t+\Delta t$, and $\Delta f_{vk,\,t+\Delta t}^{\,i-1}$ = the unbalanced force for the k-th maglev wheels to lift up the maglev vehicle.

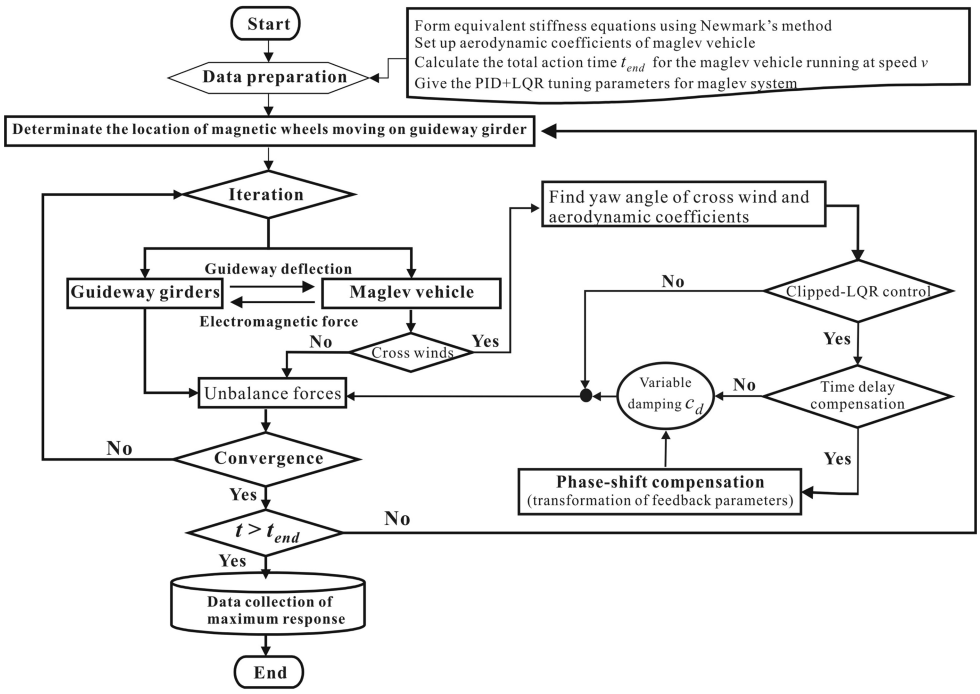

Fig. 4 Flow chat of incremental-iterative procedure

Table 1. Properties and natural frequencies of the guideway

L (m)	EI_y (kN m^2)	EI_z (kN m^2)	m (t/m)	c (kN-s/m/m)	f_{v1} (Hz)	f_{L1} (Hz)
25	5.94×10^6	1.24×10^8	1.5	15.4	5.0	22.8

f_{v1} = the first natural frequency in vertical direction, f_{L1} = the first natural frequency in lateral direction

Table 2. Properties of the maglev vehicle

l (m)	h_{z0} (m)	h_{y0} (mm)	K	m_v (kg/m)	I_T (kg-m^2)	m_w (kg)	A_S (m^2)	A_T (m^2)	d_e (m)	h_v (m)	i_0 (Ω)	R_0 (A)	Ψ_0 (Nm)
15	0.01	1	4	1200	3.8×10^5	750	52.5	52.5	0.9	1.75	25	1.0	3×10^6

8. Numerical investigations

Fig. 2 shows a maglev vehicle suspended by four magnets is traveling over a series of identical guideway girders with constant speed v. The properties of the guideway girder and maglev vehicle are listed in Tables 1 and 2, respectively. To account for the random nature and characteristics of guide-rail irregularity in practice (Shi *et al*. 2007), the following *power spectrum density* (PSD) function used by the Federal Railroad Administration (FRA) (Yang *et al*. 2004) is given to simulate the vertical profile of track geometry variations

$$S(\Omega) = \frac{A_v \Omega_c^2}{(\Omega^2 + \Omega_r^2)(\Omega^2 + \Omega_c^2)} \tag{39}$$

where Ω = spatial frequency, and A_v, (= 1.5×10^{-7} m), Ω_r (= 2.06×10^{-6} rad/m), and Ω_c (= 0.825 rad/m) are relevant parameters. Fig. 5 shows the vertical profile of track irregularity for the simulation of rail geometry variations in this study.

Because of lack of aerodynamic simulation data (from wind tunnel tests or CFD simulation) for a moving maglev vehicle, this study refers to the aerodynamic parameters measured from references (Baker 1997a,b) for a running train. The aerodynamic coefficients of side and lift forces, and moments of the maglev vehicle are linearized and approximately taken as: $C_S = C_L = 0.25\varphi$ and

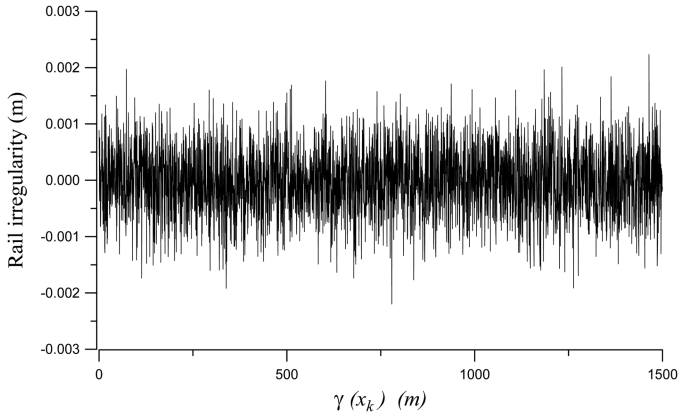

Fig. 5 Rail irregularity (vertical profile)

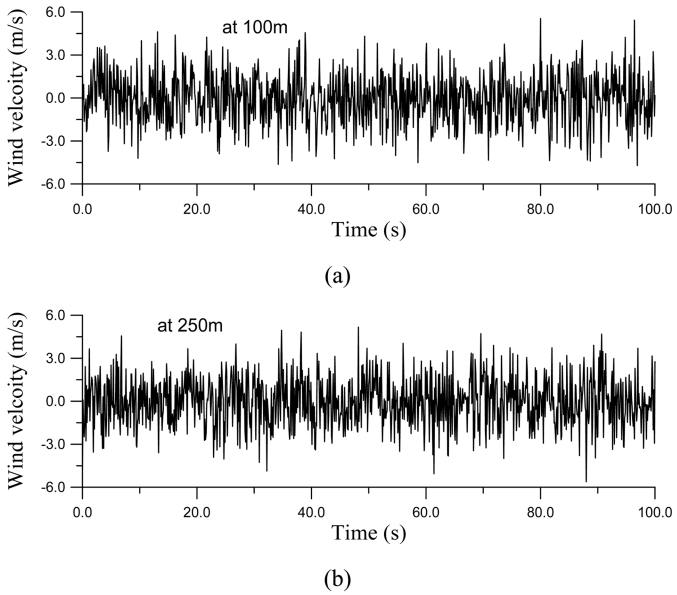

Fig. 6 Simulation of turbulent wind velocity at positions of guideway: (a) 100 m and (b) 250 m

$C_P = C_Y = 0.4\varphi$, respectively. To simulate the turbulent cross wind velocities given in Eq. (31), the following aerodynamic parameters are used: (1) the shear velocity $\overline{U}$ of the airflow is selected as 0.8 m/s; (2) the sampling number of frequency (N_f) is 1024 and the frequency increment $\Delta\omega$ is 0.006 Hz; (3) the height of the running vehicle is 6 m; (4) the time interval of the generated wind velocity is 0.1s; (5) the decay factor λ is set 10, (6) the distance l_{jn} between any two successive points is 5 m; and (7) the wind velocity field is recorded from 101 ($= N_s$) different points uniformly distributed along the guideway with the total length of 500 m. Figs. 6(a) and (b) show the generated time-histories of turbulent velocity components of cross wind with a mean velocity of $U = 20$ m/s at the positions of 100 m and 200 m from the right reference point of the guideway, respectively. As shown in Fig. 6, the fluctuating amplitudes of simulated wind speed components ($U = 20$ m/s) with time are comparable with the ones presented by Guo *et al*. (2010).

It was well known that if the *acceleration response*, rather than the displacement response, of a structure is of concern, the contribution of higher modes has to be included in the computation (Yau and Yang 2006). From the convergent verification of computed results of a simple beam under moving train loads presented in reference (Yau and Yang 2006), the first 20 modes of shape functions in Eq. (20) are sufficient to compute the acceleration response of a simple beam. In addition, the maximum accelerations of the maglev vehicle are defined as

$$a_{v,max} = max(\left|\ddot{u}_{vc} + d_k\ddot{\theta}_y\right|_{k=1,2,\ldots,K})$$
$$a_{v,max} = max(\left|\ddot{u}_{lc} + d_k\ddot{\theta}_z\right|_{k=1,2,\ldots,K}) \quad (32)$$

In the following examples, the time step of 0.001s and the ending time of $t_{end} = (NL+l)/v$ are employed to compute the dynamic response of the traveling maglev vehicle. Here, N is the span number of the guideway girders considered.

8.1. Application of the Z-N tuning rule

The purpose of this example is to determine the PID tuning parameters for the maglev vehicles running over guideway girders, thus, the aerodynamic forces acting on the moving vehicle would be excluded. As shown in Eq. (26), the linear combination of (K_p, K_i, K_d) in the PID control algorithm can provide a set of tuning gains designed for specific control process even by trial and error method. In general, if the mathematical model of a control process is not available, the *Z-N* tuning rule offers a useful approach to determine the optimal parameters of a PID controller, from which the PID parameters have been defined as (Astrom and Hagglund 1988): $K_p = 0.6K_{cr}$, $K_i = 1.2K_{cr}/T_{cr}$, and $K_d = K_{cr}T_{cr}/8$ (Ogata 1997). Here, K_{cr} means the critical proportional gain of the PID controller by increasing only the proportional control action (i.e., $K_i = K_d = 0$) K_p from 0 to a critical value K_{cr} so that the output first exhibits an oscillation behavior with a critical period T_{cr} (Ogata 1997).

Let the maglev vehicle cross the multi-span guideway with constant speed of 100 km/h. By trials for different values of the proportional gain K_p subject to $h_{zk} > 0$, the time history response of the average control error $\sum_{k=1}^{K} e_k/(K\gamma_{z0})$ to oscillate for the maglev vehicle has been plotted in Fig. 7.

In addition, the time history responses of acceleration of midpoint of the maglev vehicle and the guideway girder have been plotted in Figs. 8 and 9, respectively. As shown in Fig. 9, the increase of

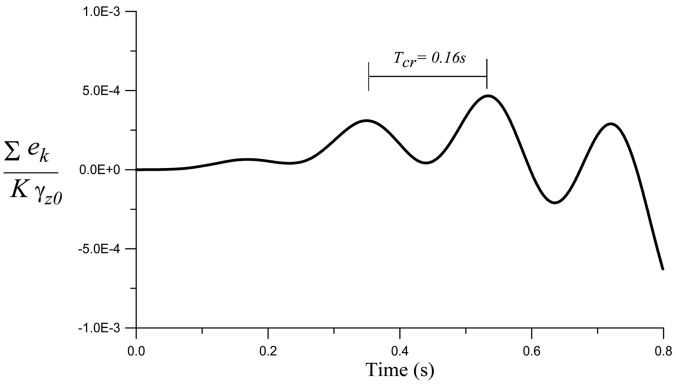

Fig. 7 Transient oscillation with a critical period T_{cr}

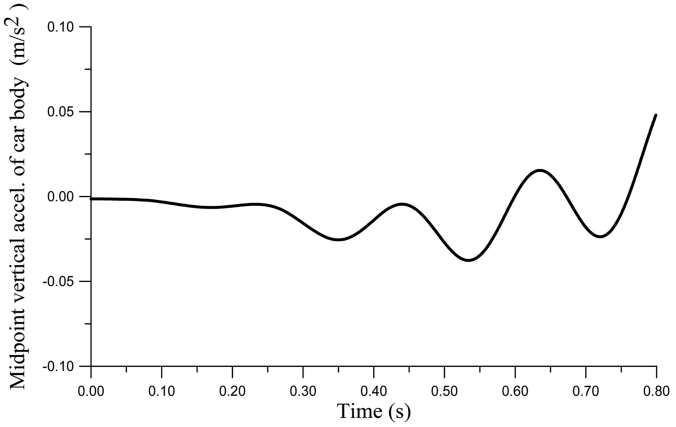

Fig. 8 Vertical acceleration of midpoint of the rigid car body

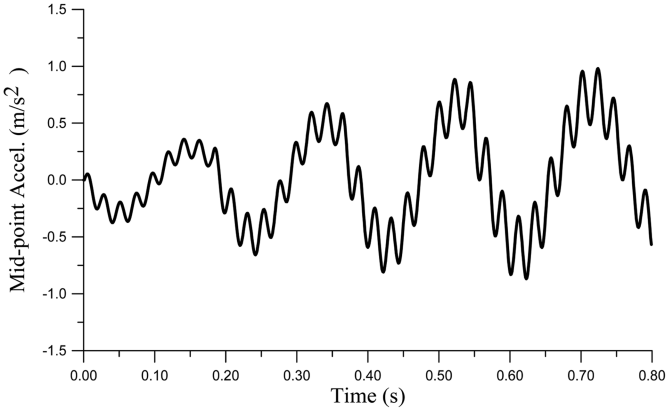

Fig. 9 Response of mid-span acceleration of the guide-way.

Table 3. Optimal PID parameters based on the *Z-N* tuning rule

K_{cr}	T_{cr} (s)	K_p (= $0.6K_{cr}$)	K_i (= $1.2K_{cr}/T_{cr}$)	K_d (= T_{cr} $K_{cr}/8$)
1.9	0.16	1.14	14.3	0.038

magnetic bogies of the maglev vehicle running into the guideway girder may lead to the response of the vibrating girder being amplified gradually. Thus, Fig. 8 indicates that the vertical acceleration of midpoint of the rigid car body increases with time. According to the *Z-N* rule described above, Table 3 has listed the corresponding optimal PID parameters. In the following examples, the optimal PID tuning parameters listed in Table 3 are used to regular the control voltage in the maglev system of the running maglev vehicle.

8.2. Maximum response analysis of maglev vehicle/guideway under cross winds

For a ground transportation system, the acceleration response of running vehicles is usually used to evaluate the ride comfort of passenger cabins and running safety of the system. For illustration, the traveling speeds of the low-speed maglev vehicle are ranged from 40 km/h to 100 km/h. With the optimal PID parameters listed in Table 3, Fig. 10 depicts the maximum acceleration ($a_{c,max}$) of the moving vehicle against various speeds (v). Such a relationship is denoted as $a_{c,max}$–v plot in the following. Fig. 11 shows the maximum acceleration (a_{max}) at midspan of the guideway girders against the moving speed (v) and this relationship will be called as a_{max}–v plot. As can be seen in Figs. 9 and 10, increasing running speeds results in the increase of acceleration amplitudes. On the other hand, let us observe the coupling effect between the lateral guidance force and the vertical levitation force (see Eq. (4)). Once the deviation of guidance gap $h_{y,k}$ increases noticeable then the levitation force (see Eq.(4(b))) would be reduced significantly. Thus the vertical response of vehicles in cross winds would become much larger than that without cross wind.

8.3 Lateral vibration control of the moving maglev vehicle

For a low speed maglev transport system, both the lateral and vertical acceleration responses of maglev vehicles are concerned with ride quality and operating safety of transportation performance.

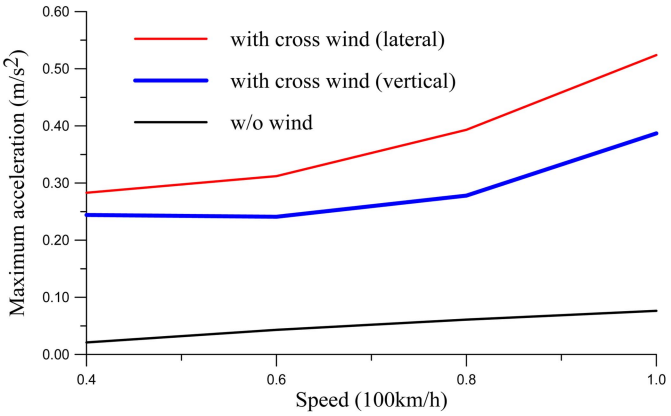

Fig. 10 $a_{c,max}$-v plot of the maglev vehicle

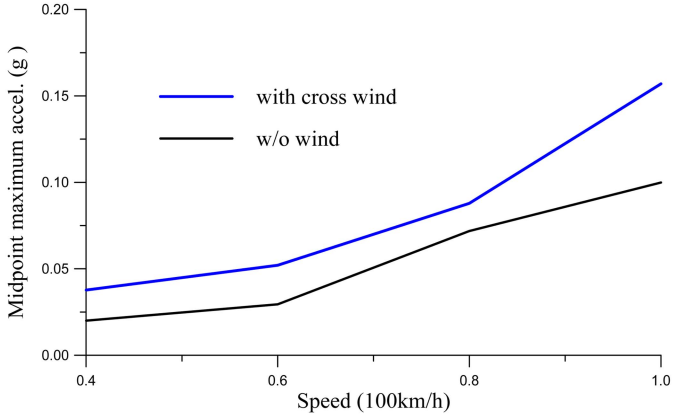

Fig. 11 a_{max}-v plot of the first span of the guideway

According to the previous numerical investigations in Section 8.2, the maximum speed of 100km/h in the $a_{c,max}$–v plot of lateral motion of the rigid car body is over the limitation of $0.05g$ (= 0.49 m/s^2) for ride requirements of passengers (Yau 2010c). In this example, we try to mitigate the vehicle's response using a PID controller in conjunction with the ideal clipped-LQR actuator presented in Section 3. Under the same cross wind environment described in Section 8.2, the corresponding lateral $a_{c,max}$–v plot for the maglev vehicle has been drawn in Fig. 12 as well. The results show that the ideal clipped-LQR actuator produces a noticeable ability to reduce the lateral vehicle's response.

8.4 Control effectiveness of clipped-LQR controller with time-delay compensation

In this example, the control effectiveness of time-delay compensation is examined for the lateral vibration of the maglev vehicle under cross winds. Let us assume the time delay τ is equal to 200 ms (micro-second). Fig. 12 shows the comparison of cross wind-induced lateral acceleration amplitudes of the moving vehicle equipped with various clipped-LQR controllers, including ideal clipped-LQR control, clipped-LQR control with time delay, and clipped-LQR control with time delay compensation. Obviously, the lipped-LQR control with time-delay degrades the control performance of the controlled system. Fortunately, with the inclusion of phase-shift compensation

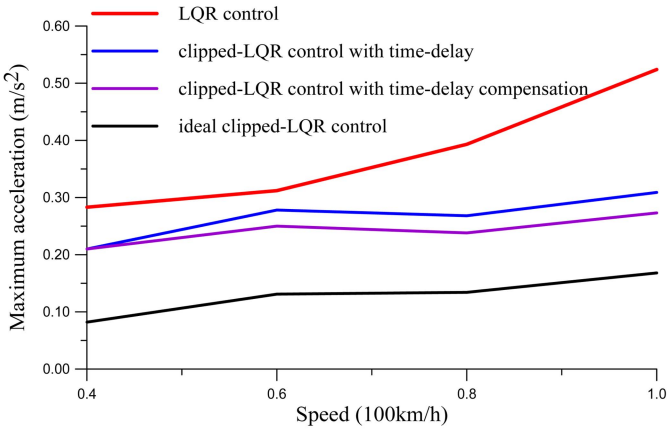

Fig. 12 Comparisons of control effectiveness

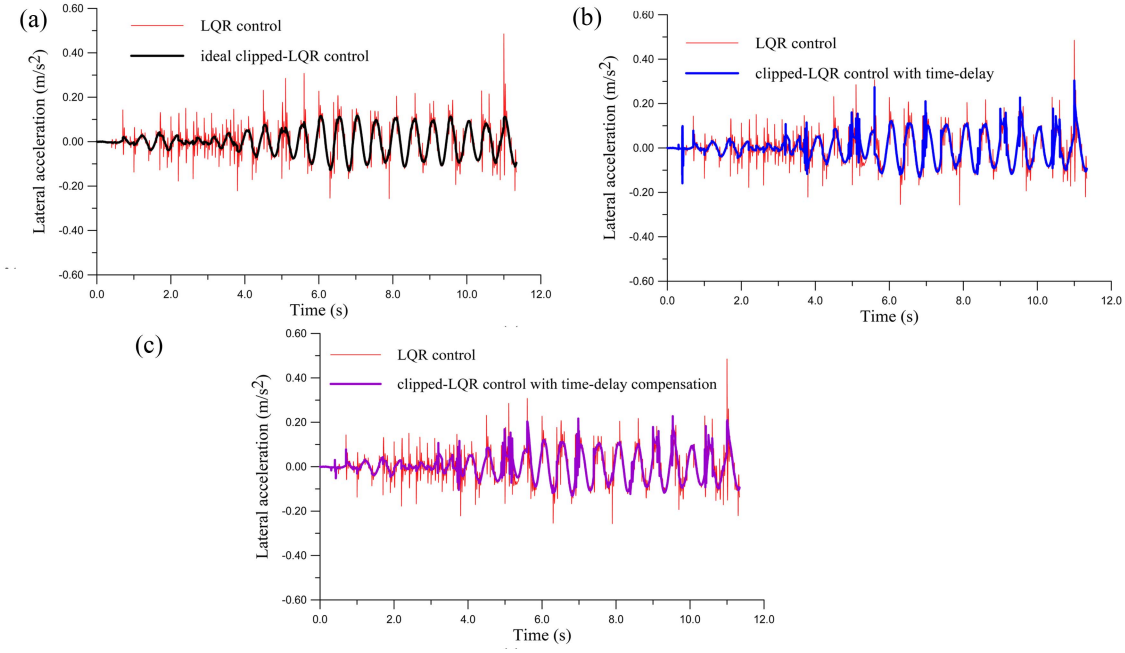

Fig. 13 Time history response of lateral acceleration of the maglev vehicle: (a) ideal clipped-LQR control, (b) clipped-LQR control with time delay and (c) clipped-LQR control with time delay compensation

method given in Section 3.2, the clipped-LQR control with time delay compensation has improved the control effectiveness. For the purpose of illustration, Figs 13(a)-(c) show the time history response of acceleration of the moving maglev vehicle installed with various clipped-LQR actuators. Obviously, the use of time delay compensation for the clipped-LQR controller produced minor improvements in suppressing the lateral response of the running maglev vehicle in cross winds.

9. Conclusions

In this study, the framework for performing nonlinear dynamic analysis and vibration control of a maglev vehicle moving over a series of guideway girders in cross winds has been conducted using an iterative approach associated with the Newmark method. Then a clipped-LQR controller with time-delay compensation is employed to control the lateral vibration of the moving maglev vehicle in cross winds. From the numerical demonstrations, the following conclusions are addressed:

1. Based on the *Z-N* tuning algorithm, the proposed PID+LQR actuator has the ability to regulate the uplift levitation and lateral guidance forces for the maglev vehicle to travel over flexible guideway girder in cross winds.
2. The aerodynamic effects of cross winds play a dominant role in affecting the lateral vibration of the maglev vehicle running over guideway.
3. With the concept of variable damping, the proposed ideal clipped-LQR controller exhibits its tuning superiority in reducing the lateral vibrations for the low-speed maglev vehicle moving in cross winds.
4. Time delay is an important issue in degrading the control performance of the present clipped-LQR controller.
5. The use of phase-shift compensation method produced minor improvements for the time-delayed clipped-LQR controller in suppressing the lateral response of the running maglev vehicle in cross winds.

Acknowledgments

The research reported herein is partly supported by grants No. NSC 99-2221-E-032-020-MY3 of *National Science Council,* Taiwan. The financial supports are gratefully acknowledged.

References

Agrawal, A.K. and Yang, J.N. (2000), "Compensation of time-delay for control of civil engineering structures", *Earthq. Eng. Struct. D.*, **29**(1), 37-62.

Aldo, D. and Alfred, R. (1999), "Design of an integrated electromagnetic levitation and guidance system for Swiss Metro", *Proceedings of the EPE'99*, Lausanne, Swiss.

Astrom, K.J. and Hagglund, T. (1988), *Automatic Tuning of PID Controllers*, Instrument Society of America.

Baker, C.J. (1991a), "Ground vehicles in high cross winds. Part I: steady aerodynamic forces", *J. Fluid. Struct.*, **5**(1), 69-90.

Baker, C.J. (1991b), "Ground vehicles in high cross winds. Part II: unsteady aerodynamic forces", *J. Fluid. Struct.*, **5**(1), 91-111.

Bittar, A. and Sales, R.M. (1998), "H_2 and H_∞ control for maglev vehicles", *IEEE Contr. Syst. Mag.*, **18**(4), 18-25.

Bocciolone, M., Cheli, F., Corradi, R., Muggiasca, S. and Tomasini, G. (2008), "Crosswind action on rail vehicles: Wind tunnel experimental analyses", *J. Wind Eng. Ind. Aerod.*, **96**(5), 584-610.

Bohn, G. and Steinmetz, G. (1984), "The electromagnetic levitation and guidance technology of the transrapid test facility Emsland", *IEEE T. Magn.*, **20**(5), 1666-1671.

Cai, Y., Chen, S.S., Rote, D.M. and Coffey, H.T. (1996), "Vehicle/guideway dynamic interaction in maglev systems", *J. Dyn. Sys. Meas. Cont.*, **118**(3), 526-530.

Cai, Y. and Chen, S.S. (1997), "Dynamic characteristics of magnetically-levitated vehicle systems", *App. Mech.*

Rev., **50**(11), 647–670.
Cao, Y., Xiang, H. and Zhou, Y. (2000), "Simulation of stochastic wind velocity field on long-span bridges", *J. Eng. Mech.- ASCE*, **126**(1), 1-6.
Fujii, K. and Ogawa, T. (1995), "Aerodynamics of high speed trains passing by each other", *Comput. Fluids*, **24**(8), 897-908.
Guo, W.W., Xia, H. and Xu, Y.L (2010), "Running safety analysis of a train on the Tsing Ma Bridge under turbulent wind", *J. Earthq. Eng*., **9**(3), 307-318.
Kwon, S.D., Lee, J.S., Moon, J.W. and Kim, M.Y. (2008,) "Dynamic interaction analysis of urban transit maglev vehicle and guideway suspension bridge subjected to gusty wind", *Eng. Struct*., **30**(12), 3445-3456.
Lee, T.Y. and Kawashima, K. (2007), "Semiactive control of nonlinear isolated bridges with time delay", *J. Struct. Eng*. -*ASCE*, **133**(2), 235-241.
Li, Y., Qiang, S., Liao, H. and Xu, Y.L. (2005), "Dynamics of wind–rail vehicle–bridge systems", *J. Wind Eng. Ind. Aerod*., **93**(6), 483–507.
Newmark, N.M. (1959), "A method of computation for structural dynamics", *J. Eng. Mech. Div*., **85**(7), 67-94.
Ni, Y.Q., Chen, Y., Ko, J.M. and Cao, D.Q. (2002), "Neuro-control of cable vibration using semi-active magnetorheological dampers", *Eng. Struct*., **24**(3), 295-307
Ogata, K. (1997), *Modern control engineering*, 3rd Ed., Prentice-Hall, Englewood Cliffs, NJ.
Samavedam, G., Kokkins, S., Raposa, F., Thompson, M. and Anagnostopoulos, G. (2002), *Assessment of CHSST Maglev for U.S. Urban Transportation*, U.S. Department of Transportation, Federal Transit Administration, Report Number FTA-MD-26-7029-2002.1.
Shi, J., Wei, Q. and Zhao, Y. (2007), "Analysis of dynamic response of the high-speed EMS maglev vehicle/ guideway coupling system with random irregularity", *Vehicle. Syst. Dyn*., **45**(12), 1077-1095.
Simiu, E. and Scanlan, R.H. (1996), *Wind effects on structures*, Wiley, NY.
Song, M.K. and Fujino, Y. (2008), "Dynamic analysis of guideway structures by considering ultra high-speed maglev train-guideway interaction", *Struct. Eng. Mech*., **29**(4), 355-380.
Soong, T.T. (1990), *Active structural control: theory and practice*, Longman Scientific & Technical, Essex, England.
Suzuki, M., Tanemoto, K. and Maeda, T. (2003), "Aerodynamic characteristics of train/vehicles under cross winds", *J. Wind Eng. Ind. Aerod*., **91**(1-2), 209–218.
Symans, M.D. and Constantinou, M.C. (1997), "Seismic testing of a building structure with a semi-active fluid damper control system", *Earthq. Eng. Struct. D*., **26**, 759-777.
Xia, H., Guo, W.W., Zhang, N. and Sunb, G.J. (2008), "Dynamic analysis of a train–bridge system under wind action", *Comput Struct*., **86**(19-20), 1845-1855.
Xu, Y.L., Zhang, N. and Xia, H. (2004), "Vibration of coupled train and cable-stayed bridge systems in cross winds", *Eng. Struct*., **26**(10), 89–1406.
Yang, Y.B. and Kuo S.R. (1994), *Theory and analysis of nonlinear framed structures*, Singapore: Prentice Hall.
Yang, Y.B., Yau, J.D. and Wu, Y.S. (2004), *Vehicle-Bridge Interaction Dynamics*, World Scientific, Singapore.
Yang, Y.B. and Yau, J.D. (2011), "An iterative interacting method for dynamic analysis of the maglev train–guideway/foundation–soil system", *Eng. Struct*., **33**, 1013-1024.
Yau, J.D. (2009a), "Vibration control of maglev vehicles traveling over a flexible guideway", *J. Sound Vib*., **321**(1-2), 184-200.
Yau, J.D. (2009b), "Response of a maglev vehicle moving on a series of guideways with differential settlement", *J. Sound Vib*., **324**(3-5), 816-831.
Yau, J.D. (2009c), "Vehicle/bridge interactions of a rail suspension bridge considering support movements", *Inter. Multisca. Mech*., **2**(3), 263-276.
Yau, J.D. (2010a), "Interaction response of maglev masses moving on a suspended beam shaken by horizontal ground motion", *J. Sound Vib*., **329**(2), 171-188.
Yau, J.D. (2010b), "Response of a maglev vehicle moving on a two-span flexible guideway", *J. Mech*., **26**(1), 95-103.
Yau, J.D. (2010c), "Aerodynamic vibrations of a maglev vehicle running on flexible guideways under oncoming wind actions", *J. Sound Vib*., **329**(10), 1743-1759.
Yau, J.D. and Yang, Y.B. (2006), "Vertical accelerations of simple beams due to successive loads traveling at

resonant speeds", *J. Sound Vib*., **289**(1-2), 210-228.
Zhao, C.F. and Zhai, W.M. (2002), "Maglev vehicle/guideway vertical random response and ride quality", *Vehicle. Syst. Dyn*., **38**(3), 185–210.
Zheng, X.J., Wu, J.J. and Zhou, Y.H. (2000), "Numerical analyses on dynamic control of five-degree-of-freedom maglev vehicle moving on flexible guideways", *J. Sound Vib*., **235**(1), 43–61.
Zheng, X.J., Wu, J.J. and Zhou, Y.H. (2005), "Effect of spring non-linearity on dynamic stability of a controlled maglev vehicle and its guideway system", *J. Sound Vib*., **279**(1-2), 201–215.

CC